JOURNAL OF CATALYSIS 54, 289–302 (1978)

The Adsorption, Desorption, and Reactions of CO and O_2 on Rh[1]

CHARLES T. CAMPBELL[2] AND J. M. WHITE

Department of Chemistry, University of Texas, Austin, Texas 78712

Received July 7, 1977; revised May 16, 1978

The adsorption and desorption of CO, O_2, and CO_2 on polycrystalline Rh have been investigated using flash desorption spectroscopy and adsorption transients. Carbon monoxide adsorbs nondissociatively on clean Rh and obeys first-order Langmuir-type adsorption kinetics with an initial sticking probability of 0.5 at 330 K. It desorbs following first-order kinetics (E_{des} = 134 kJ mole^{-1} if $\nu = 10^{13}$ sec^{-1}) at about 530 K. Oxygen adsorbs with an initial sticking probability of about 0.1. Two forms of surface oxygen are produced: one is atomically chemisorbed and quite reactive with CO; the other is perhaps a subsurface, interstitial species which requires an activation energy for reaction. These desorb as O_2 at around 1000 K. Carbon dioxide will not adsorb on Rh at 330 K. The carbon monoxide oxidation reaction on Rh has been studied using the transient kinetics of the reaction of CO gas with adsorbed oxygen and the steady-state kinetics of CO_2 production from gas phase CO and O_2. The reaction proceeds via a modified Eley–Rideal path at high temperatures, where chemisorbed CO is negligible. By this path, an impinging CO enters a mobile, transiently adsorbed precursor state with a certain probability which is a function of chemisorbed CO coverage and temperature. Once in this state the CO can visit about 15 sites before reentering the gas phase. If the oxygen coverage exceeds 0.18, CO then has almost unit probability of finding, and reacting with, an oxygen adatom at one of these sites. At lower temperature, the Langmuir–Hinshelwood path becomes important and adsorbed CO strongly inhibits oxygen adsorption.

I. INTRODUCTION

In this paper we report a study using Rh wire in which the adsorption–desorption phenomena for CO, O_2, and CO_2, and the steady-state and transient reactions producing CO_2, are studied in a single system. The results illustrate both the value and the necessity of direct comparisons of absolute quantities, such as the rate of oxygen adsorption and the overall reaction rate. Rh was chosen as the substrate because of the recent success it has enjoyed in industrial catalysis and because it has received surprisingly little attention in well-controlled surface/absorbate studies (*1–13*). Our measurements provide new information concerning the respective individual processes. These processes are both qualitatively and quantitatively similar to those on Pt and Pd, though some aspects appear unique to Rh.

These results will also serve as central background for a continuing study on Rh (*14*) in which the adsorption–desorption phenomena of NO and its reactions with CO are investigated.

II. EXPERIMENTAL

All experiments were carried out in an ion-pumped ultrahigh vacuum (UHV) apparatus (base pressure of 10^{-7} Pa) built

[1] Supported by the National Science Foundation, Grant CHE 75-13732 and the Robt. A. Welch Foundation.

[2] National Science Foundation Graduate Trainee.

0021-9517/78/0543-0289$02.00/0

of stainless steel, Pyrex, and fused silica. Reagent-grade gases were introduced through two leak valves. The UHV chamber (2.25 liters) was constructed mainly of 3.8-cm-i.d. stainless steel pipe and was connected to the ion pump with a 2.54-cm gold-sealed valve. The substrate, an ion gauge, and a line-of-sight magnetic deflection mass spectrometer (equipped with an electron multiplier) were all located in the same region of the chamber. During the catalysis experiments, the ion gauge was not operated. It was used to measure background pressures and to calibrate the mass spectrometer.

The substrate was a six-turn coil made from a 15.25-cm length of 0.051-cm-diameter polycrystalline Rh wire (99.95% purity). It was spot-welded, using tiny pieces of Pt foil as an interface, to 0.42-cm lengths of 0.018-cm-diameter tungsten wire. The latter were spot-welded to heavy Pyrex-covered tungsten rods (0.2-cm-diam). At the vacuum wall these heavy leads were connected to stainless steel feedthroughs. The substrate was heated resistively. Optical pyrometry showed that this configuration gave fairly uniform temperatures (± 25 K) over the whole coil at around 1000 K. Temperatures during experiments were deduced from applied voltage versus temperature plots which were obtained at both steady-state and flashing (5.25 K sec^{-1}) conditions with a temporarily attached thermocouple. Optical pyrometry was used as a cross-reference at high temperatures. The expected accuracy is ± 25 K and reproducibility is ± 10 K.

Three types of kinetic experiments were performed: flash desorption, transient kinetics, and steady-state kinetics. For all three the system was continuously pumped. The pumping speed was conductance limited (to minimize the effect of ion pump variation) and the time characteristic, S/V, for O_2 was 2.1 sec^{-1}.

III. RESULTS AND DISCUSSION

III.1. Sample Treatment

Initially the sample was contaminated with many carbon and nitrogen impurities which desorbed mainly as N_2 (660 K) and CO (>1000 K). After a lengthy period of high-temperature annealing (1200 K), heating in O_2 (10^{-4} Pa at 800 and above), and intermittently flashing and cooling, these carbon monoxide and nitrogen spectra were replaced with a single reproducible CO desorption peak at 530 K. This CO is caused by carbon monoxide adsorption from background gas. Pretreatment ended when reproducible results for CO desorption and CO oxidation were obtained. Afterward, a brief anneal at 1200 K removed adsorbed impurities, although occasional treatments in O_2 at 800 K were necessary.

In a separate apparatus, Auger spectroscopy on a sample of this same wire later established the reliability of this cleaning procedure. The rhodium initially contained small amounts of C, S, B, P, and Si. All except Si were readily removed by the above procedure. Interestingly, the small Si Auger signal was completely attenuated by small amounts of adsorbed CO or O. After long oxygen treatments above 800 K, the Si peak was replaced by a small oxygen impurity, which was not readily removed by heating to 1200 K or CO exposure at 800 K. It is probably related to the subsurface oxygen discussed below.

III.2. CO Adsorption–Desorption

In all flash desorption experiments, the Rh was cleaned as above and allowed to cool for about 5 min in $\sim 10^{-7}$ Pa background. After exposure, it was flash heated with a ramp that was linear (5.25 K sec^{-1}) between 400 and 850 K but not at lower or higher temperatures.

Exposure of clean Rh at 330 K to gas phase CO led to chemisorption and a single-peaked (530 K) flash desorption spectrum.

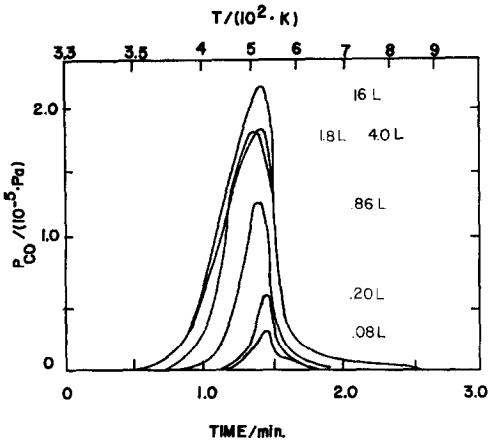

FIG. 1. Flash desorption of CO adsorbed on polycrystalline Rh wire for various exposures at 330 K. (L ≡ Langmuir = 1×10^{-6} Torr sec).

Results for exposures from 0.1 to 16 L (L ≡ Langmuir = 1×10^{-6} Torr sec) are shown in Fig. 1. The curve shape and variation of the peak position with temperature indicate a first-order desorption process (*15*). Using typical values for the preexponential factor ($A = 10^{13}$ to 10^{16} sec^{-1}) (*15, 16*) gives an activation energy for desorption, E_{des}, of 134 to 167 kJ $mole^{-1}$. This value compares to 184 kJ $mole^{-1}$, which has been reported for the heat of adsorption (*17, 18*). After exposing clean Rh to CO, CO_2 was never observed in the desorption products, even when the substrate temperature was quite high during exposure.

The variation of surface concentration (molecules cm^{-2}) with exposure at 330 K, assuming no net surface roughness, is shown in Fig. 2. Curve A was determined from flash desorption peak areas and was independent of the pressure used for the exposure. Curve B was determined by following the CO pressure as a function of time during exposure to a constant input of CO. The difference between the final steady-state CO pressure and instantaneous CO pressure, integrated from the beginning of the exposure to the time of interest, gives concentration when scaled by $S/(AkT)$. The two methods agree to within 10% at most exposures. Within experimental error the two curves can be modeled by first-order Langmuir adsorption with an initial sticking coefficient of 0.5. The maximum CO coverage of 3.4×10^{14} cm^{-2} is in reasonable agreement with previously determined values, which are around 5×10^{14} cm^{-2} (*19*).

These results are in generally good agreement with a recent study by Sexton and Somorjai (*1*), except for a high-temperature CO desorption peak (1000 K) which they observed when the Rh substrate, pretreated by heating to 600 K in 1.33×10^{-4} Pa of CO for 10 min, was exposed to 30 L of CO at room temperature and then flashed. On clean Rh, we never observed the appearance of a high-temperature peak, even when the substrate was heated to 550 K in 6.67×10^{-5} Pa of CO for 30 min. Whereas Sexton and Somorjai (*1*) suggest that CO dissociation on Rh is an important process, our data suggest the contrary. Broden *et al.* (*21*) have discussed the dissociative adsorption of CO on transition metals as a function of position in the periodic chart. Their results suggest that CO should not readily dissociate on Rh. However, Hooker and Grant (*5*) have recently cited evidence that very slight decomposition of CO may

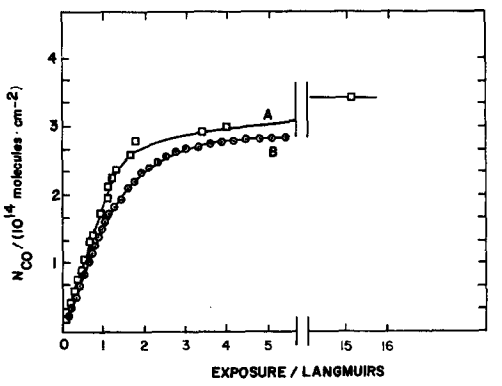

FIG. 2. Variation of CO coverage with exposure at 330 K. Curve A shows the CO flash desorption results while B shows the results of CO uptake measurements.

occur even at room temperature. Presently we do not understand the difference in the two sets of flash desorption results.

III.3. CO_2 Interactions with Rh

Exposure of clean Rh to CO_2 gas at 330 K gave no CO_2 adsorption, as judged by the CO_2 pressure during exposure and by flash desorption after exposure. Even for exposures as high as 170 L no CO_2 was observed in the flash desorption spectrum. A small CO peak was observed, but it can be fully accounted for by CO adsorption from the background. The inactivity of Rh for CO_2 adsorption has previously been reported and it is possible that detectable dissociative chemisorption can be ruled out on thermodynamic grounds (*22*). LEED results disagree on the subject of CO_2 adsorption, with one study reporting a complex diffraction pattern upon CO_2 adsorption at room temperature (*4*) while another reports rapid removal of CO_2 produced in the surface reaction of CO with adsorbed oxygen atoms (*2*). Sexton and Somorjai (*1*) report that CO_2 will adsorb on Rh. The reasons for these discrepancies are not yet clear. However, the presence of CO(g) in the background is a problem

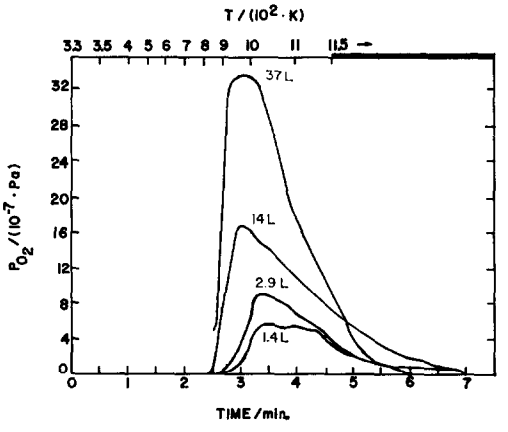

FIG. 3. Flash desorption of O_2 adsorbed on Rh for various exposures at 330 K. The temperature was constant at 1150 K after about 4.5 min into the flash experiment.

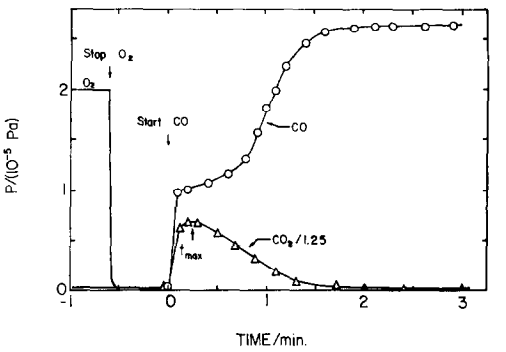

FIG. 4. Typical pressure versus time profiles for O_2, CO (○), and CO_2 (△) during a titration of chemisorbed oxygen. The O_2 exposure was 36.5 L, the O_2 pressure was 2×10^{-5} Pa, and the temperature was 330 K.

because contributions to $m/e = 28$ from CO and CO_2 cannot be easily determined. Inability to adsorb CO_2 may be related to subsurface oxygen or the sample temperature.

III.4. Oxygen Chemisorption and Reaction with Carbon Monoxide

Clean Rh at 330 K was exposed to various amounts of O_2 and, after evacuation, the flash desorption spectra showed a maximum near 1000 K, as shown in Fig. 3. This agrees with other data (*23*). The highest temperature reached in these experiments was 1150 to 1200 K. Not all of the oxygen had desorbed when this temperature was reached but the desorption rate was declining rapidly, suggesting that desorption was completed after a short anneal. This is confirmed by the subsequent CO flash desorption spectra which were characteristic of clean Rh. We have already discussed the possibility that small amounts of oxygen remained below the surface.

If CO was introduced after exposure of clean Rh to oxygen, a transient CO_2 peak, much like those in Pd (*24*) and Pt (*25*, *26*) titration experiments, was observed. The time dependence of the pressures of O_2, CO, and CO_2 is shown in Fig. 4 for a typical experiment of this type. The CO and CO_2

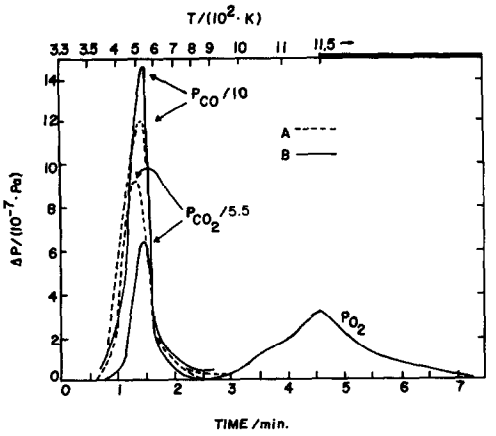

FIG. 5. Flash desorption spectra for CO, CO_2, and O_2. (A) The dashed curves were obtained by flashing after titrating a surface exposed at 330 K to 63 L of O_2 at 2.6×10^{-5} Pa. (B) The solid curves were obtained by flashing after titrating a surface exposed to 95 L of O_2 at 800 K and then cooling to 330 K. At both temperatures the O_2 pressure was 2.6×10^{-5} Pa.

pressures were usually followed simultaneously by rapid (4-sec) switching from one to the other. After the CO_2 pressure had reached the background level and the system had been evacuated, flashing the Rh gave CO and CO_2 desorption peaks as noted in Curve A of Fig. 5. As expected, the CO which had adsorbed during the previous titration desorbed around 530 K just as in the case of the pure CO/Rh system. The CO_2 desorption peaked at a slightly lower temperature (~490 K) which showed no dependence on initial oxygen coverage. Because Rh is inactive toward CO_2 adsorption at 330 K, we assume that the observed CO_2 does not arise from molecularly held CO_2 formed during the initial titration, but from an activated reaction of CO with some form of surface or near-surface oxygen.

The oxygen involved reacts very slowly at room temperature. If we assume that the oxygen participating in the initial titration is kinetically equivalent to that responsible for the CO_2 produced in the subsequent flash desorption, then the very small rate at room temperature for the latter requires a reaction order of 3.5 in oxygen coverage. Since this seems unrealistically high, we prefer to divide the oxygen into two classes: reactive (type I) and nonreactive (type II) at room temperature. This is reminiscent of recent observations on Pt (*27*) and Pd (*28, 29*) of two forms of oxygen, distinguishable on the basis of Auger, LEED, and kinetic properties.

On the basis of work function measurements (*8*), it has been suggested that a clean Rh sample at temperatures around 600 K will initially accumulate some oxygen beneath the surface upon exposure to O_2. Continued exposure gives chemisorbed oxygen above the plane of the Rh surface. The subsurface oxygen is an excellent candidate for the type II form of oxygen, especially in view of our Auger results.

Exposure of clean Rh at 800 K to 95 L of O_2, followed by cooling to 330 K in 2.6×10^{-5} Pa of O_2 and evacuation, furnished an oxygen covered surface which upon titration with CO at 330 K gave results almost identical to those achieved simply by exposure to O_2 at 330 K (Fig. 4). After titration and evacuation the Rh was flashed as before and the results are shown as curves B of Fig. 5. Compared to the results following O_2 exposure at 330 K, the CO_2 peak moved to a slightly higher temperature and a large O_2 peak appeared. Repeating this experiment, but stopping the flash at 670 K and introducing additional CO, gave an additional transient CO_2 peak. Further heating to 1150 K after this CO_2 transient gave no oxygen desorption. On this basis we conclude that the O_2 desorption peak and the transient CO_2 peak shown in Fig. 5 originate from the same oxygen source. Furthermore, we note that a significantly larger amount of type II oxygen is formed by exposure at 800 K than at 330 K and that this oxygen is readily removed by exposure to CO at elevated temperatures. We conclude that the forma-

tion of type II oxygen is an activated process. This is consistent with the formation of a subsurface species (*8*). Similar results have been noted for Pt and Pd (*28–30*). On Pd the activation energy is 70 kJ mole^{-1} (*30*), which is typical for many metals.

The surface concentrations (oxygen atoms cm^{-2}) are shown in Fig. 6 as a function of oxygen exposure of clean Rh at 330 K. Curve A shows the flash desorption results, curve B_1 the type I oxygen, and curve B_2 the type II oxygen areas. Summing B_1 and B_2 provides curve B which, like A, should be a measure of the total surface oxygen. Saturation coverage for type I surface oxygen was 2.75×10^{14} atoms cm^{-2}. Clearly, the type II oxygen (curve B_2) saturates at very low exposures and at a relatively small concentration. While there are differences between A and B accounting to as much as 50% of A at low exposure, general agreement is found. For the purpose of reaction kinetics discussed below, we can satisfactorily model these adsorption kinetics with a second-order Langmuir-type model with an initial sticking coefficient ($S_0°$) of about 0.1, although we recognize that more accurate data might necessitate a more complex model.

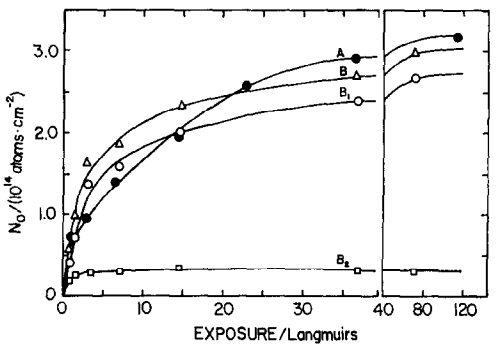

FIG. 6. Variation in the oxygen coverage with O_2 exposure at 330 K. A (●), total oxygen coverage by flash desorption; B_1 (○), reactive oxygen by CO titration; B_2 (□), nonreactive oxygen appearing as CO_2 in B; B (△), total oxygen coverage by titration ($B = B_1 + B_2$).

III.5. Kinetics and Mechanism of Oxygen Titration

On Pt, Pd, and Ir (*24–28, 30–43*) the CO oxidation reaction has generally been described in terms of some form of Langmuir–Hinshelwood (LH) or Eley–Rideal (ER) mechanism or a combination of these. Recently, the inadequacy of a simple ER mechanism, involving a direct encounter of a gas phase CO with a chemisorbed oxygen atom, has been noted (*26–28*). A better description, at temperatures and pressures where little CO chemisorbs, is provided by a model in which there is a short-lived mobile precursor state which impinging CO molecules enter with a certain probability. Once in this state, the reaction probability is almost unity, so long as the type I oxygen coverage (θ_I) lies above a certain critical value (θ^*_I), because the CO species visits many sites during its residence time at the surface. As a mathematical approximation to the more accepted precursor equation (*44*) we write this quasi-elementary reaction rate equation in the form:

$$R_{ER} = k_{ER} p_{CO} \left(\frac{\theta_I}{\theta^*_I} \right)^x, \qquad \text{(III.1)}$$

where R_{ER} denotes the Eley–Rideal rate, k_{ER} the rate coefficient for the Eley–Rideal reaction, and p_{CO} the pressure of carbon monoxide. We approximate the order (x) with respect to oxygen coverage as zero for $\theta_I > \theta^*_I$ and as unity for $\theta_I < \theta^*_I$.

When the substrate temperature is low enough and the CO pressure high enough to give measurable CO coverages in the absence of oxygen, we expect the oxidation reaction to occur (in the presence of oxygen) with important contributions from both the ER and LH paths. The latter may be written as (*25, 38, 39, 41, 42*):

$$R_{LH} = k_{LH} \theta_O \theta_{CO}, \qquad \text{(III.2)}$$

where θ_{CO} is the coverage of CO. These two

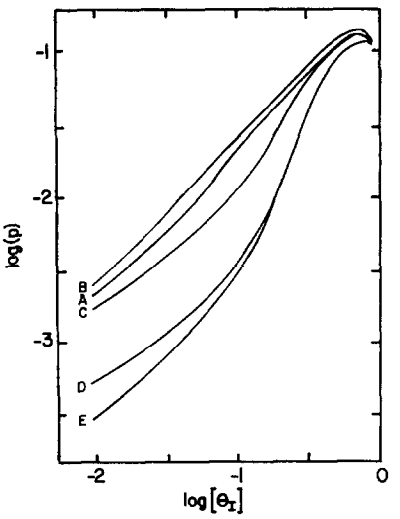

FIG. 7. Variation of the reaction probability per CO collision (p) with reactive oxygen coverage (θ_I) plotted on logarithmic scales. The data were obtained for a series of oxygen titrations at 330 K and the following nominal CO pressures: (A) 1.7×10^{-6} Pa, (B) 2.8×10^{-6} Pa, (C) 4.8×10^{-6} Pa, (D) 1.49×10^{-5} Pa, (E) 1.8×10^{-5} Pa. The initial oxygen exposure was 63 L at 2.6×10^{-5} Pa in each case.

paths represent extremes of the dynamics; in the ER case the CO is thought of as being in a two-dimensional gaseous state at the surface while in the LH case CO is in a localized chemisorbed state. Although a full description of the system requires inclusion of all the possibilities between these two extremes, division into two classes is nonetheless useful.

In order to examine the kinetics of the oxidation of carbon monoxide on Rh, we have extended measurements of the type shown in Fig. 4 over a range of initial oxygen coverages and CO pressures. At any time (t) during these titrations the CO_2 production rate could be determined from the instantaneous CO_2 partial pressure (p_{CO_2}) and the remaining type I oxygen coverage ($\theta_I(t)$) from

$$\theta_I(t) \propto \int_t^{t_e} p_{CO_2}(t')dt', \qquad \text{(III.3)}$$

where t_e is the time required to complete the transient experiment.

The reaction probability (p), defined as the ratio of the rate of CO_2 production (R_{CO_2}) to the rate of CO collisions is shown as a function of θ_I in Fig. 7. In this series of five titrations, all at 330 K where CO is readily chemisorbed, the initial oxygen coverage was near saturation, $\theta_I(t = 0) \simeq 0.9$, and the average CO pressure during a titration varied between 1.7×10^{-6} and 1.8×10^{-5} Pa. In each case we note that the maximum reaction probability occurred for $\theta_I \simeq 0.7$, i.e., well into the transient rather than at the beginning. In each titration the maximum reaction probability is about 0.13, but as the CO titration pressure increased the reaction probability at low coverages decreased. Thus, the rate of CO_2 production is first order in CO pressure at high oxygen coverage; at lower coverages the order approaches zero. The fact that the reaction probability maximizes for $\theta_I \simeq 0.7$ suggests that even at high θ_I the ER mechanism cannot account for the transient kinetic behavior and that chemisorbed CO plays an important role. For $\theta_I < 0.4$, the inadequacy of the ER path is even more obvious because of the weak pressure dependence shown by the total reaction rate. By comparing the amount of CO_2 produced with the amount of CO consumed at time t, θ_{CO} can be estimated. Measurements in the region of $\theta_I < 0.4$. indicate $\theta_{CO} > 0.4$. Assuming the CO adsorption is adequately described by a model for which the sticking probability drops as the total coverage increases, it is clear that the LH path would show an order less than unity in p_{CO}. Thus, the data in Fig. 7 are consistent with a significant LH contribution. There is also some indication that an ER contribution must be included since the rate at high oxygen coverage is very near the maximum value. If the rate were all LH, the initial rate should be very low compared to the maximum rate.

In Fig. 8 the time required to reach the maximum rate is plotted as a function of the initial oxygen coverage (θ_{Ii}) from 0.15 to near saturation. In these experiments the CO leak rate was fixed to give a final CO pressure of 2.1×10^{-5} Pa. The ER path should make its largest contribution at $t = 0$. Since the time required to reach the maximum rate is greater than the response time of the system (<10 sec) and is a decreasing function of oxygen coverage, the increasing importance of the LH contribution at lower θ_I is confirmed.

It should be noted that it was impossible to reach a fully saturated value of θ_I because the background CO pressure was always about 3% of the O_2 pressure during exposure. Assuming that oxygen adsorption is a second-order Langmuir-type process and that the reaction probability per CO collision is ~0.1 (Section III.4), the rate of use of O(a) to make CO_2 equals the rate of oxygen adsorption when the surface is 90% saturated.

The variation of the maximum reaction probability with initial coverage θ_{Ii} is shown in Fig. 9. The data are taken under the same conditions as the experiments of Fig. 8. These data show an average order in θ_{Ii} of ~0.8. Although not a direct measure of the reaction order in θ_I, they suggest

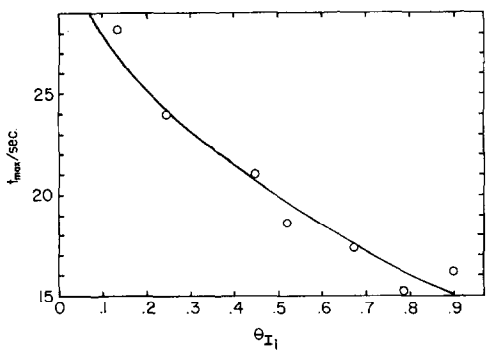

FIG. 8. Variation of the time at which the CO_2 production rate maximizes (t_{max}) with the initial oxygen coverage. The data points are for a series of titrations at 330 K in which the CO pressure after titration asymptotically approached 2.1×10^{-5} Pa.

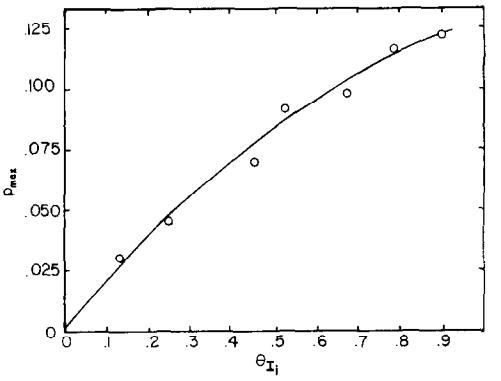

FIG. 9. The maximum reaction probability (p_{max}) as a function of the initial oxygen coverage for the series of experiments shown in Fig. 8.

an overall picture which is consistent with a model which combines the ER and LH paths.

In the context of this discussion, we should point out that Tucker (*2*) has reported that a high coverage (1.2×10^{15} atoms cm^{-2}) oxygen coincidence lattice can be formed on Rh(100) and this structure does not react with CO(g) at room T at pressures as high as 5.33×10^{-4} Pa and over times as long as several hours. At 373 K this structure reacts readily with CO(g). Tucker concluded that the reaction to produce CO_2 requires that a CO molecule first be chemisorbed next to an adsorbed oxygen atom; i.e., only the LH path is operable. This explanation seems to contradict our results.

III.6. Reaction of O_2(g) with Adsorbed CO

When CO was chemisorbed to saturation coverage at 330 K, there was no measurable increase in CO_2 pressure when 8×10^{-6} Pa of O_2 was introduced for 5 min. Furthermore, no O_2 was observed to desorb when the substrate was subsequently flashed. We conclude therefore that CO(a) strongly inhibits oxygen adsorption and that O_2(g) does not react directly with CO(a) to form CO_2. Similar behavior is well known on Pt and Pd (*24*, *25*).

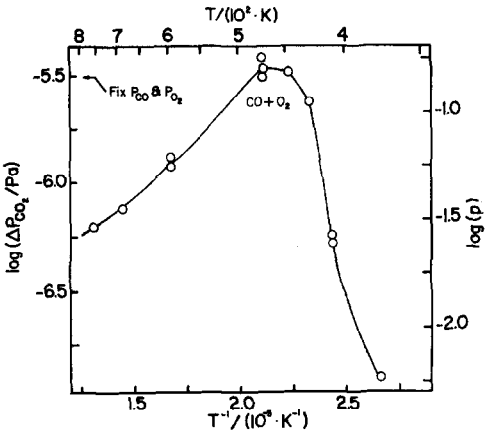

FIG. 10. Variation of the net steady-state CO_2 production rate (Δp_{CO_2}) and the reaction probability per CO collision with temperature for $p_{CO} = p_{O_2} = 3.2 \times 10^{-6}$ Pa.

III.7. Steady-State Kinetics

The steady-state rate of CO_2 production for various fixed O_2 and CO pressures was measured. Figure 10 shows the logarithm of the net rate of CO_2 production (and the logarithm of the reaction probability per CO collision) as a function of reciprocal temperature for a system in which the CO and O_2 pressures were each fixed at 3.2×10^{-6} Pa. The rate maximizes near 473 K with a reaction probability of about 0.13. Below 450 K the apparent activation energy is large (60–120 kJ mole^{-1}). Above 475 K the apparent activation energy becomes negative (~ -20 kJ mole^{-1}). At pressures near 10^{-4} Pa, Sexton and Somorjai (*1*) observed qualitatively similar steady-state data except that the peak temperature occurred at 523 K rather than 473 K. This increase in temperature required to reach the maximum rate can be understood in terms of the adsorption and desorption of CO. At higher CO pressures a higher temperature is required to lower θ_{CO} to the value which gives the maximum rate. (A more detailed discussion of this idea is given below.)

Figures 11 and 12 show logarithmic plots of the CO_2 production rate (and reaction probability) as a function of the gas phase concentration of O_2 and CO, respectively. Three temperatures, one from each of the three major regions of Fig. 10, were chosen. In Fig. 11, the CO pressure was fixed at 3.2×10^{-6} Pa. At low temperatures (410 K), where Fig. 10 indicates a positive activation energy, Fig. 11 shows the rate is first order in O_2 at low pressures but becomes zero order at higher pressures. Similar qualitative behavior is shown for the turnover region (473 K) and the high-temperature region (590 K) but the rates at a given O_2 pressure are generally quite different. The order in gas phase CO (Fig. 12) shows different qualitative behavior in the three temperature regions. At low CO pressures (relative to p_{O_2}) the rate is first order in CO pressure for all three temperature regions. At high relative CO pressures, however, the rate is inhibited by CO at low temperatures (410 K), is zero order for intermediate temperatures, and shows low but positive order at high temperatures.

In the following paragraphs we discuss the mechanism of the CO oxidation reaction on Rh. In many respects the discussion follows lines similar to those used in characterizing CO oxidation rates on Pt,

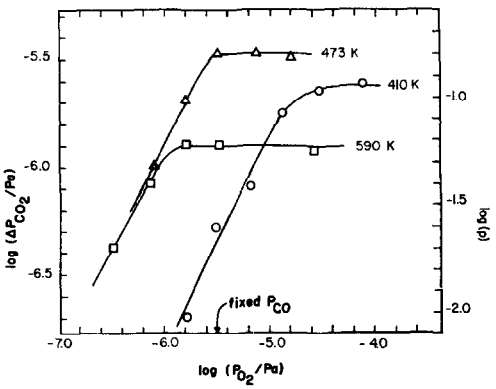

FIG. 11. Logarithmic plot of the CO_2 production rate as a function of the oxygen pressure holding the carbon monoxide pressure fixed at 3.2×10^{-6} Pa. Three fixed temperatures were used: ○ = 410 K, △ = 473 K, and □ = 590 K.

Pd, and Ir (*24–28, 30–43*). Generally, we will attempt to model the results in terms of a combination of ER and LH paths relying heavily on the transient work for support. For clarity we have divided the discussion into parts corresponding to different pressure–temperature regions.

III.7.1. $p_{O_2} \geq 0.3p_{CO}$ and $T = 590$ K. At 590 K and $p_{O_2} \geq 0.3p_{CO}$ the steady-state CO_2 production rate can be expressed as

$$R_{CO_2} = k_{590}p_{CO}, \qquad \text{(III.4)}$$

where $k_{590} = 1.7 \times 10^{17}$ molecules cm^{-2} sec^{-1} Pa^{-1}. This empirical overall rate equation implies that an impinging CO molecule incident on the surface reacts with a probability of 0.06 independent of p_{O_2}.

At this temperature and over the range of CO pressures used, the CO flash desorption data imply that only a small CO coverage will exist at steady state in the absence of oxygen. In the presence of oxygen we expect the coverage to be even smaller. The oxygen coverage is about 0.5 (see below). It is under these conditions that the ER path will predominate, if it exists. Its importance was pointed to by the transient data, and we will therefore take the view that the Eley–Rideal pathway predominates here. By comparing the reaction probability here (0.06) with that determined under similar coverage conditions by the transient method at 330 K (0.13), we see at most a weakly negative activation energy. This agrees with the view of the ER path as being essentially nonactivated on Pt and Pd (*24–28, 33*).

Consumption of O(a) through desorption as O_2 is negligible at 590 K according to the flash desorption spectra. An oxygen material balance, therefore, shows that the CO_2 production rate is equal to twice the O_2 adsorption rate at steady state. Thus the steady-state data determine an oxygen sticking coefficient of $\sim$0.030 for $p_{O_2} = p_{CO} = 3.2 \times 10^{-6}$ Pa at 590 K. Using the estimated initial sticking probability of 0.1

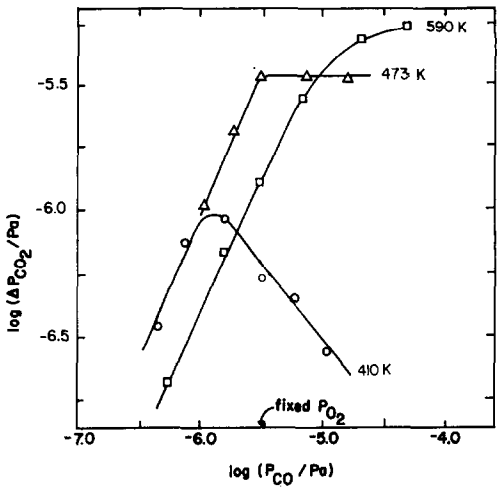

FIG. 12. Logarithmic plot of the CO_2 production rate as a function of the carbon monoxide pressure holding the oxygen pressure fixed at 3.2×10^{-6} Pa. Three fixed temperatures were used: ○ = 410 K, △ = 473 K, and □ = 590 K.

(see Section III.4) and assuming second-order Langmuir adsorption, the fraction of empty sites is about 0.5. If the O_2 pressure is increased the oxygen coverage will increase but not the CO_2 production rate; we infer that the rate is independent of θ_I, the coverage of reactive oxygen, and that a transiently adsorbed precursor must be involved in the ER mechanism. From Fig. 11 the O_2 pressure at the turnover is between 1.15 and 1.58×10^{-6} Pa. Using this figure and the reaction probability (0.06) the steady-state oxygen coverage is $0.11 < \theta_I < 0.25$. In the calculations below, therefore, we will use $\theta^*_I = 0.18$. Thus, by our approximate rate equation [Eq. (III.1)], below this coverage the rate depends on θ_I while above it the rate is determined only by the probability (0.06) of entering the mobile precursor state. [This transition actually occurs smoothly, as would be predicted by a more rigorous precursor equation (*44*)]. This suggests that on the average a CO which enters the precursor state can visit about 15 sites before reentering the gas phase. On Pt the transition coverage is about 0.5 and the

probability of entering the mobile precursor state, and thus, the reaction probability for $\theta_I \geq 0.5$, is about 0.1 (*26*). Non-unit but coverage-independent reaction probabilities imply that only a fraction of the CO molecules which impinge on the surface can enter the precursor state.

III.7.2. $p_{O_2} \geq p_{CO}$ and $T = 473$ K. When $p_{CO} = p_{O_2}$, this temperature is in the turnover region of Fig. 10. According to Figs. 11 and 12, the rate can be expressed as

$$R_{CO_2} = k_{473} p_{CO}, \qquad \text{(III.5)}$$

with $k_{473} = 4.5 \times 10^{17}$ molecules cm^{-2} sec^{-1} Pa^{-1}. That is, an impinging CO has a constant reaction probability of 0.16. The major differences between this and the 590 K expression [Eq. (III.4)] are the magnitude of k_T ($k_{473} = 2.65 k_{590}$) and the applicable pressure ranges. The smaller k_T at 590 K reflects the negative apparent activation energy over the high-temperature region of Fig. 10. The rate coefficients differ by a factor of 2.65 and according to our interpretation both regions are characterized by ER rates which are limited by the probability that an impinging CO enters the mobile precursor state. It seems intuitively reasonable that the probability of entering such a precursor state will be a decreasing function of T. This effect accounts for the high sticking probability (0.5) for CO at 330 K and the very low maximum reaction probability (0.06) at 590 K. Perhaps in the future, molecular beam studies will be able to determine the probability of entering such a presursor state as a function of surface temperature and the angle of impact. This kind of molecular level data is badly needed.

III.7.3. $p_{O_2} < 0.3\ p_{CO}$ and $T = 590$ K. For this set of conditions, the overall rate of CO_2 production is close to first order in p_{O_2} (Fig. 11). As we would expect for such a situation, the calculated coverage is always less than θ^*_I (0.18). In this situation, the overall rate is determined principally by the oxygen adsorption rate. According to Fig. 12, when p_{CO} exceeds 10^{-5} Pa, the order with respect to p_{CO} begins to decline slowly and approaches zero at 5×10^{-5} Pa. At this point the rate is very high, so high that using the procedure outlined in Section III.7.1, the estimated fraction of empty sites is 1.07 (i.e., only a tiny CO or O coverage). Apparently the rate of O_2 adsorption is near its maximum, the value reached for a clean surface, but the reaction rate is high enough to make the oxygen coverage quite low. Since the rate is O_2 adsorption limited, further increases on p_{CO} do not increase the rate.

III.7.4. $p_{CO} > p_{O_2}$ and $T = 473$ K. The rate can be expressed as

$$R_{CO_2} = k_{473} p_{O_2}, \qquad \text{(III.6)}$$

where $k_{473} = 4.5 \times 10^{17}$ molecules cm^{-2} sec^{-1} Pa^{-1}. We have not determined the order in CO pressure in the low total pressure region and k_{473} may be a function of p_{CO}. The total coverage is only about 0.1 (see method of calculation in Section III.7.1) and the rate is again determined by the oxygen adsorption rate. Adsorption processes are often essentially unactivated, and this is why the left-hand part of the 473 and 590 K curves of Fig. 11 are very close together. Notice the turnover to zero order in p_{O_2}. This turnover occurs at higher p_{O_2} at 473 K than at 590 K because of the larger ER rates available at 473 K, which keeps the oxygen coverage low at higher p_{O_2}.

At higher total pressures the order in p_{CO} is (Fig. 12) zero. Note that the rate at 473 K drops well below that at 590 K. As in Fig. 11, the saturation point at 473 K occurs at higher p_{O_2}/p_{CO} than at 590 K. Our interpretation is that the presence and effect of chemisorbed CO is pronounced in Fig. 12 whereas it is not in Fig. 11. Thus, along the high p_{CO} portion of Fig. 12, CO(a) inhibits the oxygen adsorption rate at 473 K and keeps it below the maximum value observed at 590 K. Since CO(a) is significant, it is necessary to mention the

additional effect of the LH mechanism. Our data are not sufficiently accurate at this point to ascribe the relative importances of the LH and ER paths, although a further study (*23*) will greatly help in this respect.

III.7.5. $p_{CO} > 0.3p_{O_2}$ and $T = 410$ K. The empirical rate equation in this region is

$$R_{CO_2} \propto p_{O_2}p_{CO}^{-0.6}. \qquad \text{(III.7)}$$

On the basis of the adsorption model used in Section III.7.1, the total coverage $\theta_T \geq 0.6$ in this region. Since the CO flash desorption spectra show that 410 K is just barely into the desorption region, we expect the accumulation of relatively large amounts of CO. That is, we expect impinging CO's to pass from the precursor state to a relatively long-lived chemisorbed state. The lifetime of the chemisorbed species is lengthened markedly upon lowering the temperature from 473 to 410 K because the desorption rate drops by about a factor of 200.

As compared to 573 and 473 K, the rates at 410 K and relatively low O_2 pressures are all markedly lower, indicating that a significant amount of relatively unreactive CO has accumulated. This chemisorbed CO serves to inhibit the O_2 adsorption rate, thereby inhibiting the CO_2 production rate.

At the intersection of the two linear parts of the 410 K curve of Fig. 11, the total coverage is about 0.7 and a significant fraction of this must be CO. This is large enough to make any further increases in CO serve mainly to inhibit the rate of CO_2 production as observed. Under such conditions the steady-state rate of CO_2 production is controlled by the oxygen adsorption rate and the first-order dependence on p_{O_2} is expected. Because of the facility of the LH path at 410 K on Rh (*23*), it will be important here.

III.7.6. $p_{O_2} > 3p_{CO}$ and $T = 410$ K. The steady-state rate of CO_2 production is given here by

$$R_{CO_2} = k_{410}p_{CO}. \qquad \text{(III.8)}$$

The general situation involves high coverages of oxygen, θ_I. For example, when $p_{O_2} = 9 \times 10^{-5}$ Pa and $p_{CO} = 3.2 \times 10^{-6}$ Pa, the calculated total coverage (θ_T) is 0.87. Since the rate is first order in p_{CO} and zero order in p_{O_2} we expect most of this coverage to be oxygen. If so, θ_I will be large enough to make the ER contribution to the rate be independent of p_{O_2} as observed. The rate constant, k_{410}, actually varies somewhat with pressure. For the low-pressure region (left-hand side of Fig. 12), $k_{410} = k_{473}$. At much higher pressures (right-hand side of Fig. 11), k_{410} falls 30% below k_{473}.

We must now attempt to explain why, if the ER rate is saturated in θ_I in this region, the overall rate constant at 410 K is less than or equal to that at 473 K. Our previous model for the ER rate predicts that the saturation rate at 410 K will be larger than at 473 K, reflecting an increased probability for a CO to enter the precursor state. If we assume in addition, however, that the probability of entering the precursor state decreases as a function of the coverage of chemisorbed CO, then we can understand both the smaller k_{410} and its gradual fall with pressure. This assumption is also pleasing in that, together with the large initial probability for entering the precursor state at 330 K ($\sim$0.5, per Section III.7.1), it provides an explanation for the adsorption rates observed for CO (Section III.2), while maintaining a precursor model for unification with these CO_2 data. A decreased probability could arise because of a chemical effect on the surface potential wells or a steric effect on the trajectories of the impinging molecules.

III.7.7. Temperature Dependence. The temperature dependence of the data is of considerable interest. As an example we discuss here the data of Fig. 11, in particular $p_{CO} = p_{O_2} = 3.2 \times 10^{-6}$ Pa. Below 450 K the rate is limited by oxygen adsorption because the CO coverage is high and severely limits the rate of oxygen adsorp-

tion. With increasing temperature the CO desorption rate increases rapidly, leaving empty sites which serve to increase the oxygen adsorption rate. The apparent low-temperature activation energy of 60 to 120 kJ $mole^{-1}$ reflects the activation energy for CO desorption. The inhibitory effect of adsorbed CO is gradually lost as the temperature is raised and becomes negligible when the temperature exceeds 550 K (i.e., well past the peak of the CO flash desorption spectrum). As the inhibition dies, the apparent activation energy drops rapidly. Above 425 K, the rate is characterized by an ER path since the CO coverage is very low and the oxygen coverage is high.

The desorption of oxygen as O_2 is not significant at the temperatures discussed here. The role played by the type II (nonreactive) oxygen has not been discussed here. However, its influence may be significant, especially above 473 K where conversion to the reactive form occurs readily. It may also have an effect on the catalytic activity of the Rh (*1*).

One apparent difference in the Rh data reported here and those reported for Pd (*32*) is the temperature dependence of the pressures of oxygen and carbon monoxide which exist at the turning points of Figs. 11 and 12. On Pd (*32*) such variations were not noted, although a systematic study of this point was not made. Recently, we have observed such variations on Pt (*33*) although not nearly so pronounced as on Rh. This appears to be the result of the stronger role played by the ER path in the case of Pt.

IV. CONCLUSIONS

Carbon monoxide adsorbs nondissociatively on Rh at 330 K. Based on the oxidation reaction kinetics, this adsorption is probably limited by the rate at which CO enters a mobile precursor state. The probability that a gas phase CO which strikes the surface will enter this precursor state decreases strongly with CO coverage and mildly with temperature. The kinetics of CO adsorption can be approximated by a first-order Langmuir-type equation and an initial sticking probability of 0.5 at 330 K. Chemisorbed CO desorbs following first-order kinetics at about 530 K.

Oxygen adsorbs dissociatively on Rh at 330 K, populating a reactive and a nonreactive state, with an initial sticking probability of 0.1. The reactive form of surface oxygen can be readily removed with CO at 330 K, but the nonreactive form, which probably resides under the surface, requires elevated temperatures ($\sim$490 K) for reaction. The transient reaction of adsorbed oxygen and CO(g) indicates that both the Langmuir–Hinshelwood and the Eley–Rideal pathways are significant in CO_2 production at 330 K. Surface oxygen desorbs from Rh at $\sim$1000 K.

An understanding of the rate of CO_2 production by the catalytic combination of carbon monoxide and oxygen over Rh relies heavily on a quantitative understanding of the adsorption–desorption phenomena of CO, O_2, and CO_2. For example, knowledge of the total coverage under steady-state conditions can be readily extracted from a comparison of the rate of reaction and the oxygen collision frequency, provided the initial sticking probability of oxygen is known. Also very useful is a quantitative knowledge of the CO reaction probability, for this information led directly to the concept of a mobile precursor state for CO adsorption and CO_2 production.

The carbon monoxide oxidation reaction on Rh is similar to that on Pt and Pd. At low temperatures, both the Langmuir–Hinshelwood and Eley–Rideal paths are significant. Adsorbed CO strongly inhibits the rate of oxygen adsorption and therefore reaction. At higher temperatures, the modified Eley–Rideal path predominates. It involves the reaction of a weakly adsorbed mobile CO precursor with chemisorbed oxygen. This precursor model is certainly

more pleasing from a molecular dynamic point of view than previous theories which combined the Langmuir–Hinshelwood path and a classical Eley–Rideal path. The precursor state is very closely related in an equilibrium thermodynamic sense to both gaseous and chemisorbed CO, and, as such, can be applied with advantage to situations in which both the gas phase pressure and CO coverage appear to affect the rate.

REFERENCES

1. Sexton, B. A., and Somorjai, G. A., *J. Catal.* **46**, 167 (1977).
2. Tucker, C. W., *J. Appl. Phys.* **37**, 3013 (1966).
3. Tucker, C. W., *J. Appl. Phys.* **37**, 4147 (1966); and corrections: Tucker, C. W., *J. Appl. Phys.* **38**, 2696 (1967).
4. Grant, J. T., and Haas, T. W., *Surface Sci.* **21**, 76 (1970).
5. Hooker, M. P., and Grant, J. T., *Surface Sci.* **62**, 21 (1977).
6. Barker, F. G., and Gasser, R. P. H., *Surface Sci.* **39**, 136 (1973).
7. Stewart, C. N., and Ehrlich, G., *J. Chem. Phys.* **62**, 4672 (1975).
8. Belyaeva, M. E., Kalish, T. V., and Burshtein, R. Kh., *Electrokhimiya* **9**, 546 (1973).
9. Harrod, J. F., Roberts, R. W., and Rissmann, E. F., *J. Phys. Chem.* **71**, 347 (1967).
10. Ponec, V., Knor, Z., and Cerny, S., *Coll. Czech. Chem. Commun.* **30**, 208 (1965).
11. Reid, J. U., Thomson, S. J., and Webb, G., *J. Catal.* **29**, 421, 433 (1973).
12. McKee, D. W., *J. Catal.* **8**, 240 (1967).
13. Braun, W., Meyer-Ehmsen, G., Neumann, M., Verhandl-DPG*No. 1, 1977, 348.0-73.
14. Campbell, C. T., and White, J. M., *Appl. Surf. Sci.*, in press.
15. Redhead, P. A., *Vacuum* **12**, 203 (1962).
16. Baetzhold, R. C., and Somorjai, G. A., *J. Catal.* **45**, 94 (1976).
17. Brennan, D. B., and Hayes, F. H., *Philos. Trans. Roy. Soc. (London) Ser. A* **258**, 347 (1965).
18. Kavtaradze, N. N., and Sokolova, N. P., *Dokl. Akad. Nauk.* **172**, 386 (1967).
19. The ratio of saturation O_2 adsorption to saturation CO adsorption is 1 to 1 (*20*) and therefore the CO(a) coverage is one-half the O(a) coverage. The O(a) coverage can be calculated from the data of (*2*, *3*, *6*, *10*).
20. Lanyon, M. A. H., and Trapnell, B. M. W., *Proc. Roy. Soc. (London) Ser. A* **227**, 387 (1955).
21. Broden, G., Rhodin, T. N., Brucker, C., Benlow, R., and Hurych, Z., *Surface Sci.* **59**, 593 (1976).
22. Brennan, D., and Hayward, D. O., *Philos. Trans. Roy. Soc. (London) Ser. A* **258**, 375 (1965).
23. Campbell, C. T., Shi, S.-K., and White, J. M., submitted for publication.
24. Matsushima, T., and White, J. M., *J. Catal.* **39**, 265 (1975).
25. Bonzel, H. P., and Ku, R., *Surface Sci.* **33**, 91 (1972).
26. White, J. M., and Golchet, A., *J. Chem. Phys.* **66**, 5744 (1977).
27. Matsushima, T., Almy, D. B., and White, J. M., *Surface Sci.* **67**, 89 (1977).
28. Matsushima, T., and White, J. M., *Surface Sci.* **67**, 122 (1977).
29. Conrad, H., Ertl, G., Kuppers, J., and Latta, E. E., *Surf. Sci.* **65**, 245 (1977).
30. Campbell, C. T., Foyt, D. C., and White, J. M., *J. Phys. Chem.* **81**, 491 (1977).
31. Close, J. S., and White, J. M., *J. Catal.* **36**, 185 (1975).
32. Matsushima, T., Almy, D. B., Foyt, D. C., Close, J. S., and White, J. M., *J. Catal.* **39**, 277 (1975).
33. Golchet, A., and White, J. M., to appear.
34. Matsushima, T., and White, J. M., *J. Catal.* **40**, 334 (1975).
35. Matsushima, T., Mussett, C. J., and White J. M., *J. Catal.* **41**, 397–404 (1976).
36. Becker, C. A., Corvin, J. P., Wharton, L., and Auerbach, D. J., *J. Chem. Phys.* **67**, 3394 (1977).
37. Hopster, H., Ibach, H., and Comsa, G., *J. Catal.* **46**, 37 (1977).
38. Bonzel, H. P., and Burton, J. J., *Surface Sci.* **52**, 223 (1975).
39. Engel, T., and Ertl, G., *Chem. Phys. Lett.* **54**, 95 (1978).
40. Halsey, G. D., *Surface Sci.* **64**, 681 (1977).
41. Ivanov, V. P., Boreskov, G. K., Savchenko, V. I., Egelhoff, W. F., and Weinberg, W. H., *J. Catal.* **48**, 269 (1977).
42. Zhdan, P. A., Boreskov, G. K., Egelhoff, W. F., and Weinberg, W. H., *Surface Sci.* **61**, 377 (1976).
43. Ertl, G., and Koch, J., *in* "Proceedings, Vth International Congress on Catalysis" (Hightower, Ed.), p. 969. North-Holland/Elsevier, New York, 1973.
44. Gasser, R. P. H., and Smith, E. B., *Chem. Phys. Lett.* **1**, 457 (1967).